Capturing time and vertical variability of tropospheric ozone: A study using TES nadir retrievals

Kevin W. Bowman,[1] John Worden,[2,4] Tilman Steck,[1,5] Helen M. Worden,[1] Shepard Clough,[2] and Clive Rodgers[3]

Received 29 January 2002; revised 2 May 2002; accepted 12 June 2002; published 14 December 2002.

[1] In this paper, the vertical resolution for Tropospheric Emission Spectrometer (TES) nadir ozone retrievals is established and is used to assess the ability of TES to capture time variations of ozone in the troposphere. This characterization is based on retrievals of ozone using simulated radiances generated from ozonesonde profiles taken over Bermuda from 14 April to 25 May 1993. To that end, a two-step retrieval strategy that includes an initial estimate of the "shape" of the ozone followed by a finer-resolution estimate was developed to provide rapid and robust convergence against large deviations of ozone profiles in the troposphere and lower stratosphere relative to a climatology. An error analysis is derived that accurately accounts for representation errors of the profile, choices of regularization, and the dependence of the retrieval error on both the statistics of the profile and spectral measurement noise, as well as the sensitivity of these retrievals to errors in temperature. This analysis shows that TES should be able to retrieve ozone in the nadir with an approximately 6 km resolution in the troposphere. The root-mean square errors in estimates of the upper and lower tropospheric columns are about 1.35 Dobson units (DU) each. With this vertical resolution, TES would have the sensitivity to detect both the enhanced and reduced tropospheric ozone present in the Bermuda data set. Coupled with a 2-day near-repeat orbit and global coverage, TES retrievals of ozone could provide invaluable information to distinguish between anthropogenic and meteorological sources for the time variability of ozone in the troposphere. *INDEX TERMS:* 0365 Atmospheric Composition and Structure: Troposphere—composition and chemistry; 3260 Mathematical Geophysics: Inverse theory; 3359 Meteorology and Atmospheric Dynamics: Radiative processes; 3360 Meteorology and Atmospheric Dynamics: Remote sensing; 3394 Meteorology and Atmospheric Dynamics: Instruments and techniques

Citation: Bowman, K. W., J. Worden, T. Steck, H. M. Worden, S. Clough, and C. Rodgers, Capturing time and vertical variability of tropospheric ozone: A study using TES nadir retrievals, *J. Geophys. Res.*, *107*(D23), 4723, doi:10.1029/2002JD002150, 2002.

1. Introduction

[2] The Tropospheric Emission Spectrometer (TES) on the EOS-Aura spacecraft will measure the global 3-dimensional distribution of ozone in the troposphere and many of the chemical species that are part of its formation and destruction. Global remote sensing measurements, along with in situ data and atmospheric models, are needed to address key questions related to the Earth's lower atmosphere [*Roscoe and Clemitshaw*, 1997; *Singh and Jacob*, 2000]. In particular, TES measurements will contribute to the understanding of the sources of ozone in the troposphere with implications for climate change, the oxidizing capacity of the atmosphere, and air quality on a global scale [*Crutzen*, 1995; *Wang and Jacob*, 1998].

[3] TES is an infrared Fourier Transform Spectrometer (FTS) with both limb and nadir sounding capabilities [*Beer et al.*, 2001]. TES will record the Earth's spectral radiance from discrete locations along the orbit track in the wave number range 650 to 2250 cm^{-1} (15.4 to 4.4 μm). The standard products that will be retrieved from these spectra are vertical concentration profiles of ozone, water vapor, carbon monoxide, methane, nitric oxide, and nitric acid.

[4] In this paper, we will study whether TES nadir measurements are sensitive enough to capture the ozone time variability using spectra simulated from a set of real ozone measurements. To that end, we have acquired a set

[1]Jet Propulsion Laboratory, California Institute of Technology, Pasadena, California, USA.
[2]Atmospheric and Environmental Research, Cambridge, Massachusetts, USA.
[3]Oxford University, Oxford, UK.
[4]Now at Jet Propulsion Laboratory, California Institute of Technology, Pasadena, California, USA.
[5]Now at Forschungszentrum Karlsruhe, Institut für Meteorologie und Klimaforschung, Karlsruhe, Germany.

0148-0227/02/2002JD002150$09.00

of 15 ozonesonde profiles from the Bermuda station (32°N latitude, 64°W longitude) [*Oltmans et al.*, 1996; J. Logan, data set obtained from private communication, 2000] taken between 13 April and 27 May 1993. These profiles were chosen because of their considerable variability in the troposphere. In particular, several of the ozonesonde profiles show enhanced ozone concentrations in the upper troposphere. The temporal spacing of these ozonesondes, which were taken approximately every other day, also provides a reasonable simulation of the TES temporal sampling. TES will have a near repeat view (separated by about 1° longitude) of its nadir targets every 2 days.

[5] The estimation or "retrieval" of the vertical ozone profiles is based on an iterative minimization of the difference between a "measured" spectrum and a "model" spectrum subject to constraints that ensure a physically plausible solution. The "measured" spectra are calculated with the ozonesonde profiles and predicted TES measurement noise. The "model" spectra are calculated with estimates of the ozone profiles. This iterative process is nonlinear and can be computationally expensive. We improve the convergence rate by using a two-step algorithm that is based on a coarse vertical resolution estimate of an ozone profile followed by a fine resolution estimate [*Clough et al.*, 2002]. An analysis of errors for this algorithm characterizes the representation errors of the profile, choice of regularization, and the dependence of the retrieval error on both the statistics of the profile and spectral noise. This error analysis is used to determine the resolution of the retrievals and their sensitivity to time variations in the ozone profiles.

[6] The retrievals of ozone vertical distributions based on simulated measurements establish the theoretical limits that can be obtained from TES nadir spectra. These limits become a baseline for characterizing the impact of systematic errors in actual TES retrievals as well as providing a means of assessing the scientific utility of TES nadir ozone retrievals.

2. TES Description

[7] The EOS-Aura spacecraft is expected to be launched in January 2004 into a Sun-synchronous orbit at 705 km altitude, with a nominal 1345 LT equator crossing time. TES is one of four instruments on this platform that will study the chemistry of the troposphere and lower stratosphere. The other instruments are the Microwave Limb Sounder (MLS) with microwave radiometers, the High Resolution Dynamics Limb Sounder (HIRDLS), an infrared scanning radiometer, and the Ozone Measuring Instrument (OMI) that employs UV grating spectrometers. See http://aura.gsfc.nasa.gov/ for details on the Aura mission. As an infrared FTS, TES measures spectrally resolved emission features from atmospheric trace gases that are subsequently used to infer vertical concentration profiles of those trace gases. In its limb mode, the 16 detectors elements on TES will simultaneously measure spectra from the surface to about 33 km, with fields of view that are around 2.3 km high and 23 km wide. Because the limb mode has long lines-of-sight (around 200 km in the tangent layer) through the atmosphere, TES will be sensitive to species with low concentrations, such as NO and HNO_3. For TES nadir views, the detectors have a combined footprint that covers 5.3 by 8.4 km. Because of the lower probability of cloud interference, the nadir mode will provide better global coverage of the troposphere than the limb mode for the more abundant species of O_3, H_2O, CO and CH_4. However, in the nadir mode, vertical information is obtained only from spectral variations along the line-of-sight as opposed to the vertical information available from detectors imaging different altitudes in the limb viewing geometry. Because of this, sufficient spectral resolution and signal-to-noise ratio are required to distinguish between stratospheric and tropospheric infrared signatures. TES spectral resolution was chosen to match the average pressure-broadened widths of weak infrared molecular transitions in the lower troposphere for nadir measurements (0.1 cm^{-1}, apodized) and in the upper troposphere for limb measurements (0.025 cm^{-1}, apodized) [*Beer et al.*, 2001]. The current strategy for TES observations is to operate in a "Global Survey" mode every other day, with "off" days reserved for special observations such as off-nadir views of volcanoes, biomass burning events, correlative measurement campaigns, and additional calibration tests. On the Global Survey days, limb and nadir measurements must alternate with calibration measurements of the on-board blackbody and views of cold space for radiometric offset and slope determination. A sequence of 2 calibration scans, 2 nadir scans, and 3 limb scans allows 73 sequences per orbit with target observations spaced just under 5° along the orbit track.

3. Retrieval Problem

3.1. Forward Model and Generation of Radiances

[8] The TES forward model [*Clough et al.*, 1995; *Beer et al.*, 1999] solves the equation of radiative transfer for a specified atmospheric state. The resulting spectral radiance is integrated with the field-of-view functions and convolved with the instrument line shape to produce an estimate of the radiance that would have been measured by TES. Under clear sky conditions, the modeled radiance for the nadir (downlooking) mode includes three contributions: upwelling atmospheric emission, attenuated reflected downwelling atmospheric emission and attenuated surface emission. For this study, we neglected reflected solar radiation, which has an insignificant contribution to radiances in the 9.6 μm band. Optical depths are calculated using temperature-interpolated absorption coefficients precomputed on a fixed pressure grid. The absorption coefficients were calculated using LBLRTM (line-by-line radiative transfer model) [*Clough and Iacono*, 1995] with the HITRAN96 database [*Rothman et al.*, 1998] modified to include updated water vapor line parameters [*Toth*, 1998; *Toth et al.*, 1998]. Absorption due to the water vapor continuum is also included in the optical depths [*Clough et al.*, 1989; *Clough*, 1995].

[9] The ozonesonde profile set includes temperature, H_2O, and O_3. These quantities are mapped onto a vertical grid that is equally spaced in log pressure similar to the UARS pressure grid (http://hyperion.gsfc.nasa.gov/Analysis/UARS/uars.html). This mapping ensures that the integrated

ozone column amounts between pressure levels are consistent with the column amounts on the original ozonesonde altitude grid. The ozonesonde profiles only take measurements up to 10 hPa. However, because TES is sensitive to ozone concentrations up to around 0.1 hPa, it is necessary to incorporate a realistic ozone profile between 10 and 0.1 hPa. A URAP ozone climatology profile (http://hyperion.gsfc.nasa.gov/Analysis/UARS/urap/home.html) for the upper stratosphere is combined with the Bermuda ozonesonde profiles to create a composite ozone profile defined from the surface to 0.1 hPa. However, the results of the study are only shown up to 10 hPa, or approximately 30 km. While pressure levels were used for all of the computations, the figures in this study have been displayed as a function of altitude.

[10] For this simulation (1) we assume that surface temperature, atmospheric temperature, and water amount have been accurately retrieved prior to the ozone retrievals. However, systematic errors from the retrieval of temperature are discussed in section 4.1.2. (2) The spectral range of the retrieval is $\nu \in [985, 1075]\text{cm}^{-1}$ and the spectrum is unapodized. (3) Gaussian white noise with a standard deviation of $\sigma = 0.132$ mw/m^2 sr/cm^{-1} is added to the simulated radiances. This noise level is a conservative estimate compared to the predicted values for TES [*Beer et al.*, 2001] and is designed to partially account for the effect of systematic errors on the accuracy of the retrievals. (4) The surface temperature for all profiles is set to 290 K. (5) All of the retrievals are performed under clear sky conditions. Therefore, the accuracy of these retrievals provide an upper bound on the actual performance of TES under normal seeing conditions. (6) Systematic errors associated with the instrument calibration, instrument line shape, or molecular line parameters are not included in our error analysis. These systematic errors are important; however, our perspective is that the high spectral resolution of TES, in conjunction with multiple cross-comparisons with other satellite, ground-based, and aircraft measurements, will allow for mitigation and accurate characterization of these types of errors.

3.2. Retrieval Approach

[11] Measured radiances in TES can be related to a forward model through the following additive noise model:

$$\mathbf{y} = \mathbf{F}(\mathbf{x}, \mathbf{b}) + \mathbf{n} \tag{1}$$

where $\mathbf{y} \in \mathbb{R}^{\mathrm{N}}$, which is a real vector of length N, is the calibrated, measured spectrum; $\mathbf{x} \in \mathbb{R}^{\mathrm{M}}$ is the "full" state vector whose elements are the natural log of the volume mixing ratio (vmr) of ozone defined on a log pressure grid and $\mathbf{b}$ is a vector containing all the other trace gases, atmospheric temperature profile, geometry of the spacecraft, etc. necessary to define the radiative transfer from the atmosphere to the space craft. The vector $\mathbf{b}$ will be dropped in the subsequent derivations because these parameters are fixed for the purpose of the retrievals. The forward model $\mathbf{F} : \mathbb{R}^{\mathrm{M}} \rightarrow \mathbb{R}^{\mathrm{N}}$ simulates a spectrum produced from the propagation of radiation through the atmosphere from the Earth to the spacecraft. The noise term $\mathbf{n} \in \mathbb{R}^{\mathrm{N}}$ is assumed to be zero-mean, Gaussian white noise so that $\mathbf{S}_n = E[\mathbf{n}\mathbf{n}^{\top}] = \sigma^2\mathbf{I}$, where $E[\cdot]$ is the expectation operator [*Papoulis*, 1984] and σ is the standard deviation of the noise defined in section 3.1.

[12] The full state vector contains the natural log of the volume mixing ratio of ozone discretized on equidistant log pressure values that correspond to approximately 0.8 km in altitude. This fine discretization is chosen to accurately model the radiative transfer through the atmosphere. Through this approximation, the spectral radiance at the satellite can be calculated by numerically solving the radiative transfer equation using these layers as described in section 3.1. While this fine discretization is necessary to accurately model the radiative transfer, the vertical structure present in the full state vector can not be retrieved in the nadir mode. In order to regularize the retrieval, a retrieval vector is defined that constrains the possible values of the full state vector. The retrieval vector and the full state vector are related by a linear mapping:

$$\mathbf{x} = \mathbf{M}\mathbf{z}, \tag{2}$$

where $\mathbf{z} \in \mathbb{R}^{\mathrm{M}'}$ is the retrieval vector and $\mathbf{M} \in \mathbb{R}^{\mathrm{M}\times\mathrm{M}'}$ is a mapping matrix. We use two kinds of mapping. The first is the shape retrieval, which is based on the approach described by *Clough et al.* [2002]. This mapping is constructed to retrieve the broad features of the ozone profile such as the mean and gradient of ozone in the troposphere as well as the peak and width of the stratospheric ozone shape. The second is linear interpolation in volume mixing ratio as a function of log pressure. This interpolation is represented as a piecewise linear function with the segments connected at "nodes." The elements of $\mathbf{z}$ are the nodes of this piecewise linear function. Because these nodes are referenced to specific forward model levels, they are also referred to as retrieval levels. This mapping is designed to capture the finer resolution details of the ozone profile.

[13] The first step in the retrieval approach is the shape retrieval, which constrains the retrieval by the use of its restricted mapping from retrieval parameters to forward model levels. This estimate is then used as the initial guess for the second step. The second step is a fine resolution, "level" retrieval that is based on a piecewise linear function with 26 nodes. The level retrieval is regularized with a Twomey-Tikhonov-type smoothing constraint matrix, Λ. The construction of this constraint and its strength relative to the data is described by *Steck and Clarman* [2001] and *Steck* [2002].

[14] The two-step retrieval is summarized as follows:

$$1.\quad \hat{\mathbf{x}}_s = \mathbf{M}_s \cdot \min_{z_s} \| \mathbf{y} - \mathbf{F}(\mathbf{M}_s\mathbf{z}_s) \|^2_{\mathbf{S}_n^{-1}} \tag{3}$$

$$2.\quad \hat{\mathbf{x}} = \mathbf{M} \cdot \min_{z} (\| \mathbf{y} - \mathbf{F}(\mathbf{M}\mathbf{z}) \|^2_{\mathbf{S}_n^{-1}} + \| \mathbf{z} - \mathbf{z}_c \|^2_{\Lambda}) \tag{4}$$

where $\mathbf{M}_s$ is the mapping matrix for the shape retrieval, $\mathbf{z}_s$ is the retrieval vector for the shape retrieval, $\mathbf{M}$ is the mapping matrix for the level retrieval, $\mathbf{z}$ is the retrieval vector for the level retrieval, and $\mathbf{z}_c$ is retrieval constraint vector, and $\mathbf{S}_n$ is the error covariance matrix defined above. The initial guess for equation (4) is

$$\mathbf{z}_0 = \mathbf{M}^*\hat{\mathbf{x}}_s, \tag{5}$$

where **M*** is the pseudo-inverse of the level mapping matrix. A more detailed description of the cost functions in equations (3) and (4) and the numerical methods needed to solve them are described in Appendix A.

3.3. Error Analysis

3.3.1. Error Analysis for the Estimated Profile

[15] The error analysis for the moderately nonlinear case, i.e., where the forward model is linear over the domain of the retrieval errors, is based on the following linear estimate of the retrieval [*Rodgers*, 2000]:

$$\hat{\mathbf{x}} = \mathbf{x}_c + \mathbf{A}_{xx}(\mathbf{x} - \mathbf{x}_c) + \mathbf{M}\mathbf{G}_z\mathbf{n}, \tag{6}$$

where **M** is the mapping matrix defined in equation (2), the measurement noise vector **n** is defined in equation (1), **x** is the true full state vector (the ozonesonde profiles), the constraint state vector, $\mathbf{x}_c = \mathbf{M}\mathbf{z}_c$, is fixed for the ensemble of retrievals, $\mathbf{G}_z$ is the gain matrix, which is defined by

$$\mathbf{G}_z = \left((\mathbf{K}\mathbf{M})\mathbf{S}_n^{-1}(\mathbf{K}\mathbf{M})^\top + \Lambda_z\right)^{-1}(\mathbf{K}\mathbf{M})^\top\mathbf{S}_n^{-1}, \tag{7}$$

where

$$\mathbf{A}_{xx} = \mathbf{M}\mathbf{G}_z\mathbf{K} \tag{8}$$

is the averaging kernel. The matrix **K** in equations (7) and (8) is the Jacobian, which is defined by

$$\mathbf{K} = \frac{\partial \mathbf{F}(\mathbf{x})}{\partial \mathbf{x}}. \tag{9}$$

The averaging kernel may be interpreted from equation (6) as the sensitivity of the retrieval to the true state, i.e., $\mathbf{A}_{xx} = \partial\hat{\mathbf{x}}/\partial\mathbf{x}$.

[16] Equation (6) becomes the basis for the calculation of the second-order statistics of the retrieval and its error. The mean of the estimate is

$$E[\hat{\mathbf{x}}] = \bar{\hat{\mathbf{x}}} = \mathbf{x}_c + \mathbf{A}_{xx}(\bar{\mathbf{x}} - \mathbf{x}_c), \tag{10}$$

where the noise is assumed to be a zero-mean measurement noise vector and $\bar{\mathbf{x}} = E[\mathbf{x}]$. The covariance is

$$\mathbf{S}_{\hat{\mathbf{x}}} = \mathbf{A}_{xx}\mathbf{S}_\mathbf{x}\mathbf{A}_{xx}^\top + \mathbf{M}\mathbf{G}_z\mathbf{S}_n\mathbf{G}_z^\top\mathbf{M}^\top \tag{11}$$

where $\mathbf{S}_{\hat{\mathbf{x}}} = E[(\hat{\mathbf{x}} - \bar{\hat{\mathbf{x}}})(\hat{\mathbf{x}} - \bar{\hat{\mathbf{x}}})^\top]$ and

$$\mathbf{S}_\mathbf{x} = E[(\mathbf{x} - \bar{\mathbf{x}})(\mathbf{x} - \bar{\mathbf{x}})^\top] \tag{12}$$

is the covariance of the state vector **x**.

[17] The error in the estimate of the atmospheric profile is

$$\tilde{\mathbf{x}} = \mathbf{x} - \hat{\mathbf{x}}. \tag{13}$$

Substituting equation (6) into equation (13) leads to

$$\tilde{\mathbf{x}} = \underbrace{(\mathbf{I} - \mathbf{A}_{xx})(\mathbf{x} - \mathbf{x}_c)}_{\text{smoothing error}} + \underbrace{\mathbf{M}\mathbf{G}_z\mathbf{n}}_{\text{noise error}}. \tag{14}$$

[18] Equation (14) bears some discussion. The error vector is composed of two terms. The latter term transforms the random spectral error into an error on the full state vector. Hence, this term is called the retrieval noise error. The first term results from applying constraints to the estimate of the ozone. These constraints can be a combination of "hard" constraints, e.g., representing the profile on a coarse pressure grid, or "soft" constraints, e.g., adding the quadratic penalty function in equation (A5) to ensure an acceptable regularization. This term is the so-called "smoothing" error [*Rodgers*, 2000]. Physically, the smoothing error describes the extent to which a remote observing system is sensitive to fine vertical structure as defined, in this context, on the forward model grid. An important consideration for the smoothing error is the grid on which it is defined. The proper grid is the one from which the radiances and hence the residuals are calculated, i.e., the forward model grid, because both the true state and the estimate are referenced to this grid. An advantage of this approach is that estimates based on retrieval parameters, e.g., the shape retrieval, can be characterized in the same way as more "traditional" hard constraints, e.g., "level" retrievals.

[19] The mean of the error vector is

$$E[\tilde{\mathbf{x}}] = \bar{\tilde{\mathbf{x}}} = (\mathbf{I} - \mathbf{A}_{xx})(\bar{\mathbf{x}} - \mathbf{x}_c) \tag{15}$$

assuming a zero-mean measurement noise vector. The total error covariance matrix is

$$\mathbf{S}_{\tilde{\mathbf{x}}} = (\mathbf{I} - \mathbf{A}_{xx})\mathbf{S}_\mathbf{x}(\mathbf{I} - \mathbf{A}_{xx})^\top + \mathbf{M}\mathbf{G}_z\mathbf{S}_n\mathbf{G}_z^\top\mathbf{M}^\top, \tag{16}$$

where $\mathbf{S}_{\tilde{\mathbf{x}}} = E[(\tilde{\mathbf{x}} - \bar{\tilde{\mathbf{x}}})(\tilde{\mathbf{x}} - \bar{\tilde{\mathbf{x}}})^\top]$. It is important to note that in order to calculate the smoothing error and consequently the total error covariance, the covariance of the true state vector, **x**, must be known. This knowledge is particularly important when the smoothing error is the dominate term in the total error. For this study, ozonesondes taken over Bermuda from 1993 to 1996 were used to calculate the climatological or "true" covariance (J. Logan, private communication, 2000). In addition, we also calculated the covariance of the ensemble of test ozonesondes profiles. This covariance is used to compare the statistics of the ozonesondes to the climatology and to validate the error analysis of the retrievals.

3.3.2. Application to Error Analysis of Column Calculations

[20] In section 4.2, we estimate column abundances for the upper and lower troposphere from the estimates of the profiles over the whole troposphere. These column abundances are calculated by first converting the profile in volume mixing ratio into number density and then integrating in altitude over the region of interest. This operation can be expressed algebraically as

$$\hat{\mathbf{c}} = \mathbf{h}^\top\mathbf{x}, \tag{17}$$

where $\hat{\mathbf{c}}$ is the estimated column and $\mathbf{h} \in \mathbb{R}^M$ is the column operator, which includes both the vmr conversion and integration over the vertical region of interest, e.g., 7–15 km. The linear estimate of the column becomes

$$\hat{\mathbf{c}} = \mathbf{c}_c + \mathbf{a}_h^\top(\mathbf{x} - \mathbf{x}_c) + \mathbf{h}^\top\mathbf{M}\mathbf{G}_z\mathbf{n}, \tag{18}$$

where $\mathbf{a}_h^\top = \mathbf{h}^\top\mathbf{A}_{xx}$.

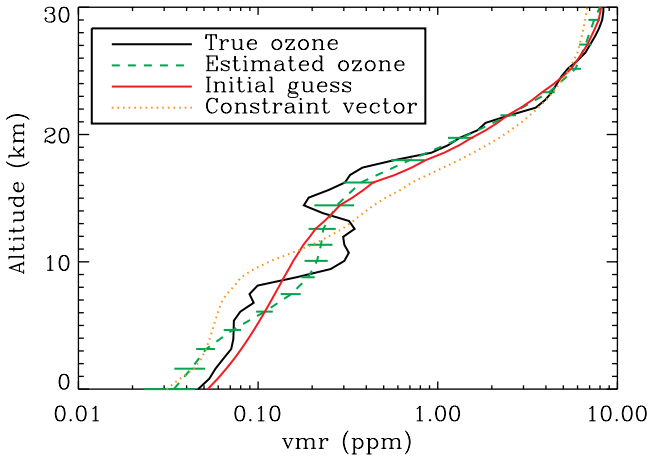

Figure 1. Retrieval of the 30 April ozonesonde profile. The figure shows the profile taken from the ozonesonde, the estimate of the ozone profile, the initial guess profile (the estimate from the shape retrieval), and the constraint profile (taken from climatology). The location of the retrieval levels are indicated by the error bars.

[21] The errors associated with the column estimate are calculated by transforming the error covariance of the retrieval. This transformation can be expressed as

$$\sigma_{\tilde{\mathbf{c}}}^2 = (\mathbf{a}_h^\top - \mathbf{h}^\top)\mathbf{S}_\mathbf{x}(\mathbf{a}_h - \mathbf{h}) + \mathbf{h}^\top \mathbf{S}_n \mathbf{h}, \tag{19}$$

where $\tilde{\mathbf{c}} = \mathbf{h}^\top \tilde{\mathbf{x}}$ is the column error.

4. Results

[22] The two-step retrieval technique described in section 3.2 was used estimate vertical ozone profiles associated with each of the 15 Bermuda ozonesonde profiles. In order to understand the effect of the vertical and temporal variability of these Bermuda profiles on the ozone estimates, we examine in detail the retrievals of the 30 April and 5 May ozonesonde profiles, which have significantly different vertical characteristics. In particular, the 30 April ozonesonde profile has a layer of enhanced ozone at 11 km (220 hPa) [*Oltmans et al.*, 1996]. These retrievals are characterized by their resolution and the accuracy of the estimate relative to the estimated standard deviation of the total error. This analysis is then extended to the ensemble of retrievals where the assumptions in the error analysis can be tested.

[23] The ability of TES to capture time variations in ozone is intimately tied to the vertical scales of those variations. We determine the resolution of the retrieval in the TES nadir mode. With this information, we examine the ozone time series over the appropriate vertical scales and discuss their role in understanding mechanisms of the time variability of ozone over Bermuda.

4.1. Ozone Retrieval Results

4.1.1. Retrieval of 30 April and 5 May 1993 Ozone Profiles

[24] Figure 1 shows 30 April 1993 ozonesonde profile, the estimate from the shape retrieval, and the estimate from the level retrieval. The location of the nodes of the level retrieval are indicated by the error bars.

[25] The shape retrieval was performed by minimizing the maximum likelihood (ML) cost function described in equation (A1) starting with the initial guess from the shape retrieval. Only one iteration was necessary. The linear decrease with logarithmic pressure of the ozone profile between 15 and 25 km was captured by the shape retrieval estimate. A robust estimate of this part of the profile is critical because the level retrieval tends to converge slowly for a poor initial guess in this region [*Clough and Iacono*, 1995; *Clough et al.*, 2002]. The estimate from the shape retrieval was then used as an initial guess for the level retrieval. The constraint vector was calculated from climatology [*Logan*, 1999]. The level retrieval was performed by minimizing the augmented ML cost function described in equation (A5). The level retrieval converged in 3 iterations. The convergence criteria were satisfied when the norm of the weighted-residual in equation (A3) was near unity and the total change in the ratio between the norm of the step-size and the norm of the retrieval vector at the last iteration was less than 0.1%. The level retrieval improves the shape retrieval estimate of the enhanced ozone volume mixing ratio between 9 and 15 km. However, the final estimate is unable to completely resolve the ozone feature in this range. In the lower troposphere, the level retrieval overestimates the ozone profile between 5 and 9 km and then underestimates the ozone profile from the surface to 5 km.

[26] The resolution of the retrieval is characterized by the averaging kernel, which is defined from equation (8) as the sensitivity of the estimate to perturbations in the true state. As described in section 3.3.1, this averaging kernel incorporates effect of both the "hard" and "soft" constraints on the retrieval. Selected rows of the averaging kernel matrix for the 30 April level retrieval case are shown in Figure 2. Each row indicates the relative contribution of each element of the true state vector to the estimated state vector at a particular altitude (or pressure) level. The vertical resolution for the retrieval is characterized by the width (or full-width-

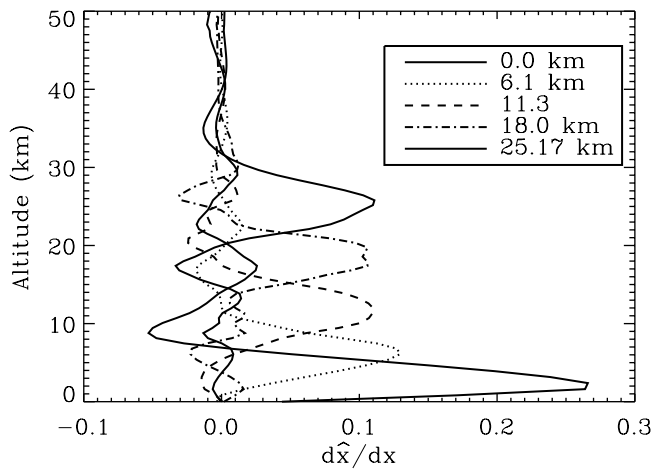

Figure 2. Averaging kernel calculated for the retrieval of the 30 April ozonesonde profile. Each line corresponds to the change in the ozone estimate from a change in the true ozone at the specified altitude.

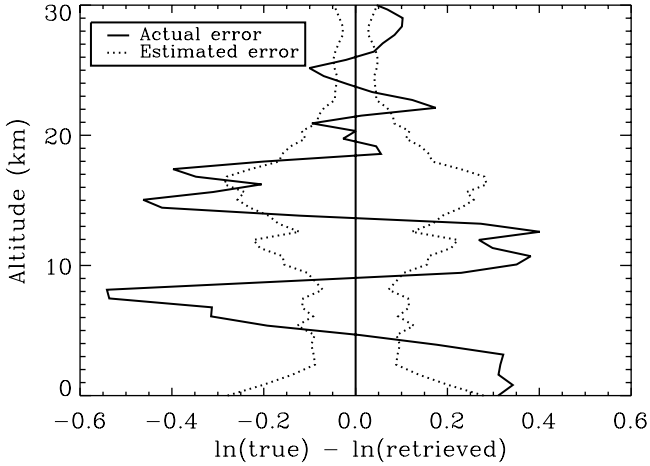

Figure 3. The estimated retrieval error along with the error between the 30 April ozonesonde profile and retrieved ozone profile.

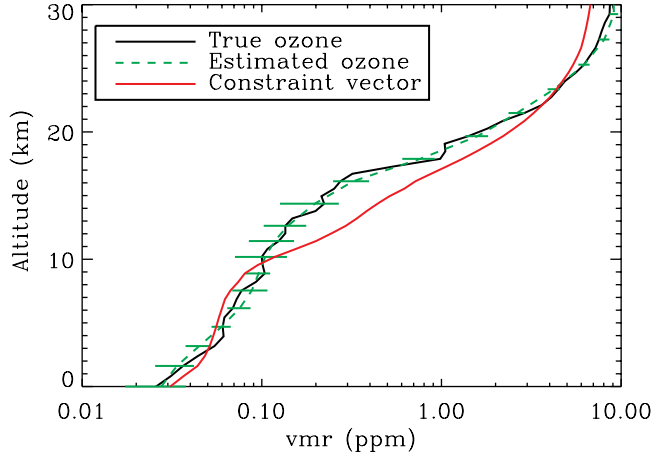

Figure 4. Retrieval of ozone for the 5 May ozonesonde profile. The location of the retrieval levels is indicated by the error bars.

half-height) of each row [*Rodgers*, 2000]. For the troposphere, this resolution is about 6 km. Hence, the estimate of the logarithm of ozone at 11.3 km is effected primarily by changes in the true state from roughly 8 km to 15 km. As a result, this resolution indicates that estimates of the ozone in troposphere are generally unaffected by variations in ozone in the stratosphere. The enhanced ozone layer centered around 12 km is about 6 km in width, which is at the resolving limit of the retrieval. Consequently, we would expect to accurately estimate the integrated column abundance of the enhanced layer but not any of its features. Figure 2 also shows that the retrieval at the surface is primarily sensitive to variations in ozone from 1 to 4 km with the peak at 2.5 km. The ozone estimates in the boundary layer are particularly sensitive to thermal contrast and humidity. TES retrievals should be more sensitive to variations in ozone deeper in the boundary layer under dryer conditions than were present in the Bermuda data set where the water vapor was typically 2% of the air at the surface.

[27] The error bars shown in Figure 1 are taken as the square-root of the diagonal values of the total error covariance in equation (16). Figure 3 shows the estimated total error and the actual error between the retrieved and true profiles. Above 30 km, the errors are not particularly meaningful because the stratosphere is fixed to the UARS climatology. The error in the estimate at 8 km is significantly greater than expected from the error bars. Nevertheless, the estimated error is consistent with the error in the ensemble of retrievals, as discussed in section 4.1.3. This indicates that 30 April ozone profile has a greater vertical variability than the other profiles in the data set.

[28] In contrast to the 30 April profile, the 5 May profile exhibits much smoother vertical characteristics. The estimate of the level retrieval is depicted in Figure 4 along with the true profile. The constraint vector was again taken from climatology. The level retrieval captures the linear component of the profile below 12 km. The error between the retrieval and the true ozone is shown in Figure 5. In contrast to the 30 April case, the actual error is generally less than the expected deviation, but the error around 4 km is approximately 3σ, which is comparable to the 0 April case.

4.1.2. Sensitivity of Retrieval to Temperature Errors

[29] The retrieval of the 30 April ozone profile, along with the other retrievals, assumed perfect knowledge of the temperature profile. In order to examine the effect of errors in temperature on the ozone retrieval, the temperature profile for 30 April was retrieved based on minimizing the augmented ML cost function in equation (A5) with a Twomey-Tikhonov-type constraint over the spectral range of $\nu \in [665,711]\text{cm}^{-1}$. The strength of the constraint was calculated in the same manner described by *Steck* [2002]. The initial guess for the temperature retrieval was chosen to be the average over all the temperature profiles in the data set. Gaussian white noise with a standard deviation of $\sigma = 1.18 \times 10^{-2}$ W/m^2/sr/cm^{-1} was added to account for the measurement noise. The absolute root-mean-square (rms) error in the temperature retrieval was less than 1 K with a mean resolution of approximately 3.7 km. The error from the temperature was propagated into the ozone retrieval, i.e., the retrieved temperature rather than the true temperature was used for the forward model calculations. The effect of

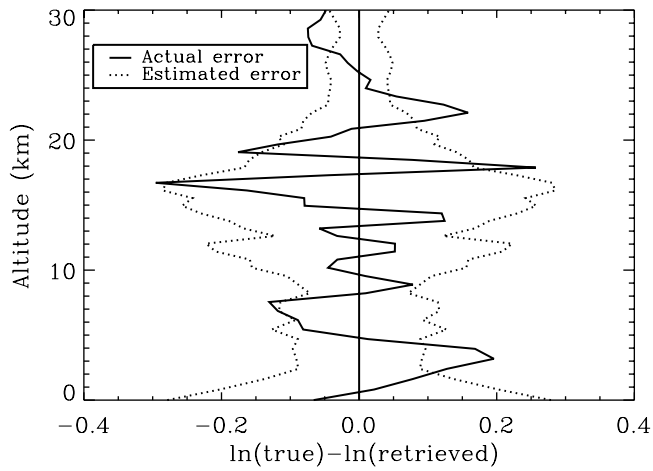

Figure 5. Error in the retrieval of 5 May 1993 ozonesonde profile.

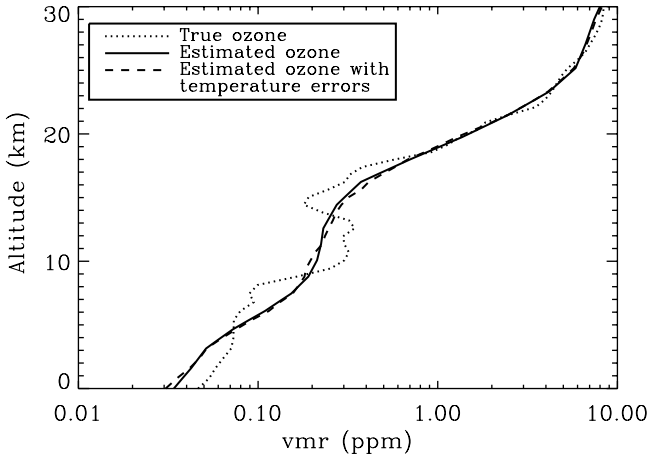

Figure 6. Comparison of 30 April ozone retrieval with and without temperature errors.

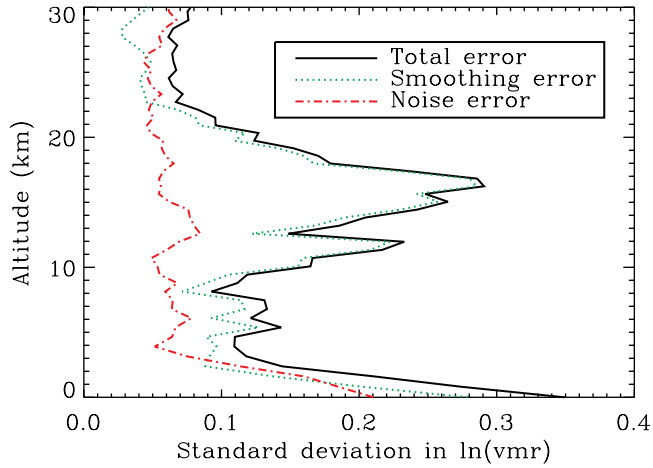

Figure 7. The estimated standard deviation of the total, smoothing, and retrieval noise error in the ozone estimate calculated from the 30 April retrieval.

temperature error on the 30 April ozone retrieval is shown in Figure 6. The standard deviation of the percentage error from 0 to 50 km between the true and estimate ozone is 21.5% whereas the percentage error between the estimated ozone and the estimated ozone with temperature errors is 4.5%. These results suggest that temperature errors of less than 1 K do not significantly affect the accuracy of the ozone retrievals.

4.1.3. Error Analysis Over an Ensemble of Profiles

[30] The importance of the vertical variability of ozone in the accurate assessment of the errors in the retrieval is underscored by significant differences in accuracy in the estimates of the ozone profiles in Figures 3 and 5. As a result, the validity of the error analysis must be tested over an ensemble of profiles. The errors in the retrieval are a function of the vertical variability, which is described statistically as $\mathbf{S_x}$, through the smoothing error, which is defined in equation (14), and related to the total error in equation (16). Figure 7 shows the relative contribution of the standard deviation of the smoothing and retrieval noise error to the estimated standard deviation of the total error. This error is defined in terms of "fractional error," which is the difference between the logarithm of the ozonesonde and estimated profiles; the term is derived on the approximation $\delta \ln \mathbf{x} \approx \delta\mathbf{x}/\mathbf{x}$ for small $\delta\mathbf{x}$. For a 0.8 km grid, Figure 7 shows that the smoothing error is the dominant term in the total error from approximately 6 km to 24 km. Hence, the accuracies of these retrievals of ozone in the mid-to-upper troposphere are limited by the vertical resolution of the retrieval and are a function of the vertical variability of the ozone.

[31] The estimated standard deviation of the smoothing and total error describes the errors for an ensemble of retrievals. The validity of this estimate is based on the assumption that the retrievals are linear or moderately nonlinear [*Rodgers*, 2000] and that the first and second-order moments of the probability distribution function (pdf) exist for the state vector [*Papoulis*, 1984]. We can test these assumptions by comparing the error covariance calculated from the ozonesonde and retrieved profiles to the estimated error covariance calculated for one retrieval, which we have selected to be the 30 April case. This comparison for the standard deviation of the error is shown in Figure 8. The standard deviation of the "empirical" total error is calculated from the difference between the ozonesonde and retrieved profiles whereas the estimated standard deviation of the total error is calculated from equation (16). Two estimated total error covariance matrices are calculated for comparison. The first one uses a climatological covariance matrix, which is calculated from Bermuda ozonesonde profiles between 1993 and 1996. The second total error covariance matrix (the "ensemble" total error covariance matrix) uses a "climatological" covariance matrix that is calculated from the test ozonesonde profiles only. The difference between the ensemble total error covariance matrix and the empirical error covariance matrix is much less than the absolute value of the total error itself,

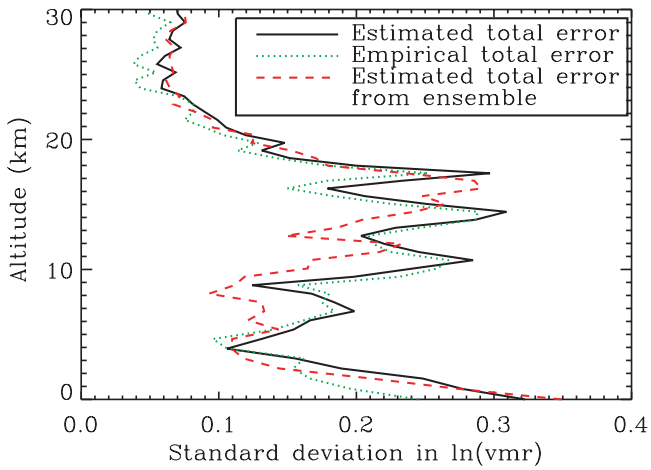

Figure 8. Comparison between the standard deviation of the "empirical" total error, the ensemble total error, and the estimated total error (from climatology). The standard deviation of the empirical total error is calculated from the difference between the ozonesonde and retrieved profiles. The ensemble total error is calculated from the error analysis using the ensemble of profiles for the climatology whereas the estimated total error is calculated using a more realistic climatology.

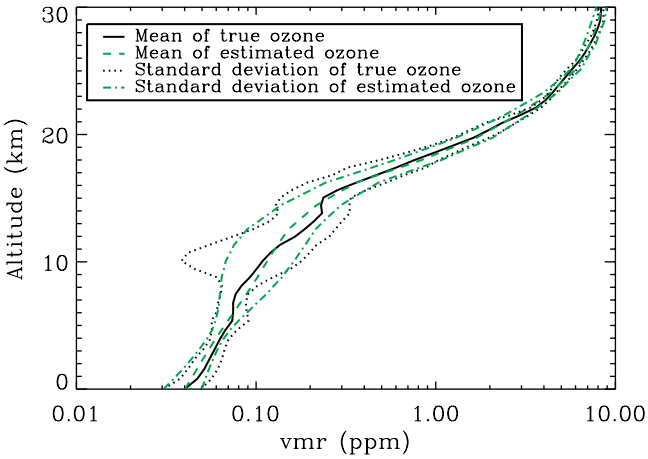

Figure 9. The standard deviation and mean of the ensemble of ozonesonde profiles and the retrieved ozone profiles.

which suggests that the assumptions for the error analysis are valid. In addition, the ensemble total error covariance compares well with the estimated total error covariance that used climatology. This agreement furthermore suggests that this data set is reasonably representative of the climatology.

4.2. Ozone Time Variability

[32] Statistical techniques are frequently used to characterize the time variability of ozone. However, this characterization needs to take into account the principal physical processes that control the temporal evolution of ozone. Over timescales of weeks where meteorological forces dominate, the time variation of ozone at a specific location is not well described by Gaussian statistics. Nevertheless, a monthly variance at a given latitude and longitude [e.g., *Logan*, 1999], is a useful, albeit incomplete, description of ozone time variability. Figure 9 show the standard deviation of the retrieved profiles along with the mean and standard deviation of the ozonesonde profiles calculated over a month. The variation of the ozonesonde profiles in the troposphere about their mean ranged from around 10% at 5 km to 65% at 11 km. The variance of the retrieved profiles is consistent with the variance of the ozonesonde profiles except from 9 to 12 km. The variation of the retrieved profiles reached 40% about their mean for this altitude range. Ozone variations in this data set are strongest around the tropopause and the vertical ozone structure have typical length scales of 6 km or less around the tropopause. The discrepancy in the statistics between the ozonesondes profiles and the retrieved profiles at a 0.8 km resolution is due to the smoothing error, which is a function of the high vertical variability of the enhanced ozone events in the data set and the resolution of the retrieval. As the variability of the ozone increases, the smoothing error as well as the total error will increase.

[33] While the absolute error in the estimate increases with the variability of the true profiles, the relative error of the time variability of the retrieved profiles to the time variability of the true profiles is approximately constant. This relationship is derived from equation (11), which equates the covariance of the retrieval to the sum of the covariance of the true profiles filtered by the averaging kernel and the covariance of the retrieval noise. In the case where the retrieval noise is negligible compared to the smoothing error covariance, the ratio of the retrieved covariance to the true covariance may be written as

$$\mathbf{S}_{\mathbf{x}}^{-1}\mathbf{S}_{\hat{\mathbf{x}}} \approx \mathbf{S}_{\mathbf{x}}^{-1}\mathbf{A}_{xx}\mathbf{S}_{\mathbf{x}}\mathbf{A}_{xx}^{\top}. \tag{20}$$

For the case of a highly variable atmosphere where $\mathbf{S}_{\mathbf{x}} = \beta\mathbf{I}$ (β is a positive scalar), equation (20) becomes

$$\mathbf{S}_{\mathbf{x}}^{-1}\mathbf{S}_{\hat{\mathbf{x}}} \approx \mathbf{A}_{xx}\mathbf{A}_{xx}^{\top}. \tag{21}$$

In this case, the relative error from (21) is only a function of the averaging kernel. In the more general case of equation (20), the fractional covariance is invariant to any scalar increase in the variability of the atmosphere.

[34] The 6 km vertical resolution suggests that we have approximately two "pieces of information" in the troposphere. One way of displaying this available information is to compare ozonesonde and retrieved column amounts for the upper and lower troposphere. The troposphere is subdivided from 0.0 to 7.5 km and from 7.5 km to the tropopause. This separation is convenient because the ensemble of profiles shows a "node" at 7.5 km that varies little with time. This node, however, may be an artifact of the data set and therefore not representative of tropospheric ozone generally. The column amounts are then computed for these two altitude ranges. The tropopause heights are determined using criteria from *Bethan et al.* [1999] and are shown in Figure 10. These column amounts are shown in Figure 11. The RMS error of the upper troposphere is 1.37 Dobson units (DU) and 1.34 DU in the lower troposphere. The mean fractional error in the column estimates is 1% for both the upper and lower troposphere and the standard deviations of the fractional error of the column estimates are on average 7.5% in the upper troposphere and 4.8% in the lower troposphere. The error in the column estimate is expressed through equation (19), which only differs from equation (16) by the choice of the averaging kernel. If the column estimate is within the vertical resolution of the retrieval, then we would expect that the relative contribution of the smoothing error to the total error to be much less than for the error of the volume mixing ratio over the altitude region on which the column is calculated. Figure 7 shows the standard deviations of the total, smoothing, and retrieval noise error for the profile retrieval of ozone. In the upper troposphere, the relative contribution of the variance of the smoothing error to the total error variance is approximately 90%. In the lower troposphere, the relative contribution of the smoothing error is on average 60%. For the calculation of the column, the relative contribution of the smoothing error to the variance of the total error is 60% in the upper troposphere and 20% in the lower troposphere.

[35] Clearly, the ability of TES to capture time variations of ozone is critically dependent on the vertical scales of interest for ozone. At roughly 1 km vertical resolution, the error in the estimate of the time variations of ozone at 12 km is almost 30%. At 6 km vertical resolution, however, the error in the upper tropospheric column drops to 7.5%. The estimate of ozone at this resolution and error is sufficient to study mechanisms that control the temporal

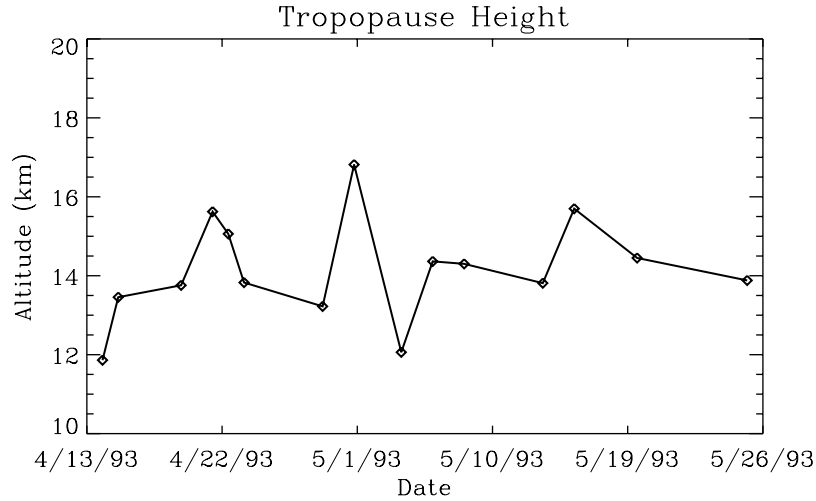

Figure 10. The calculated tropopause height for each ozone profile.

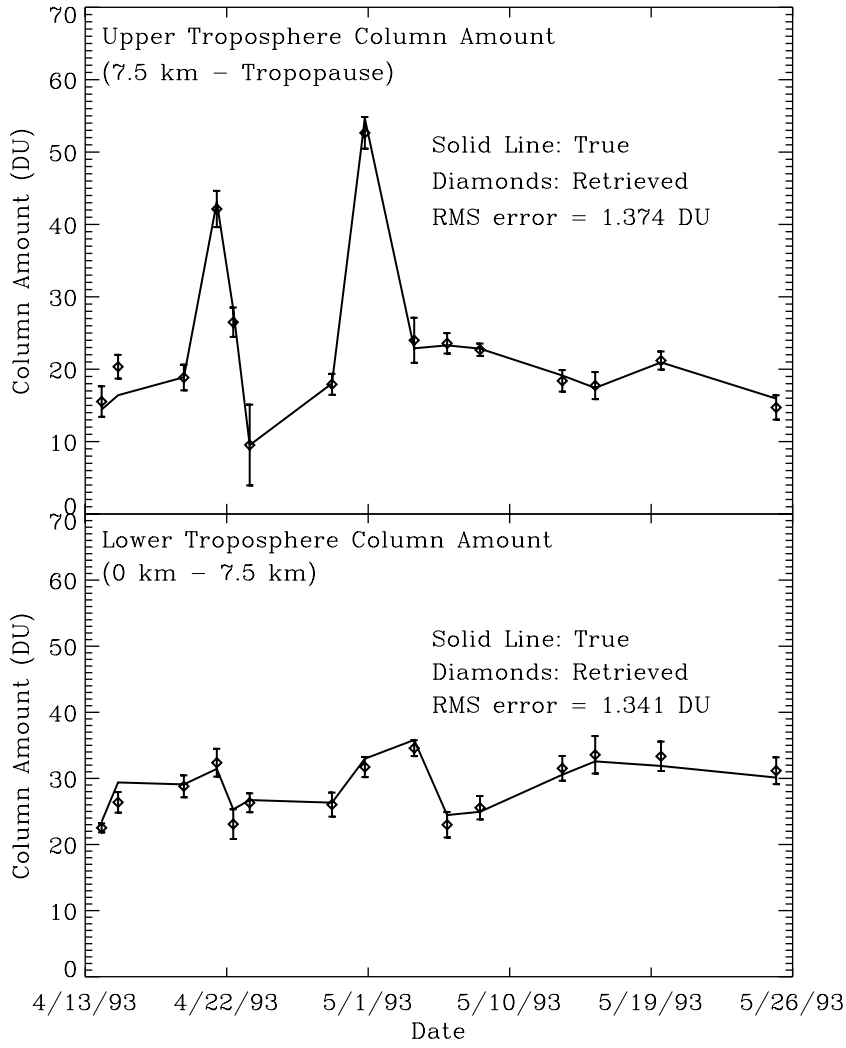

Figure 11. Column time series of the upper and lower troposphere. The solid lines represent the ozonesonde column and the diamonds represent the estimated columns.

variation of ozone in the troposphere. In particular, TES would have the sensitivity to detect the enhanced ozone events in the troposphere seen at Bermuda during the North Atlantic Regional Experiment (NARE) [*Fehsenfeld et al.*, 1996]. The enhanced events on 21 April and 30 April and the reduced ozone on 23 April are clearly shown in Figure 11. During the NARE campaign the changes from large to small ozone concentrations occurred on the order of 3–6 days, which is within the TES temporal sampling frequency. These enhanced ozone events can come from anthropogenic sources off of Northern America as well as stratospheric loading [*Moody et al.*, 1995; *Browell et al.*, 1996]. Both causes are a function of meteorological transport [*Moody et al.*, 1996; *Merill et al.*, 1996]. The spatial sampling of TES (M. Lou et al., Simulated observation of tropospheric ozone and CO with the Tropospheric Emission Spectrometer (TES) satellite instrument, submitted to *Journal of Geophysical Research*, 2002), which can measure outflow from North America as well as ozone distributions in the North Atlantic, and the ability to simultaneously estimate stratospheric ozone, temperature and humidity should provide invaluable information on distinguishing the sources of time variability of ozone in the troposphere.

5. Summary

[36] The sensitivity of TES nadir ozone retrievals to temporal variations in ozonesonde profiles measured over Bermuda from 14 April 1993 to 25 May 1993 has been investigated. The temporal sampling of the profiles corresponds approximately to the TES near-repeat orbit. The data set included enhanced ozone events in the upper troposphere. We developed a robust, two-step retrieval approach to estimate the ozone profiles. This two-step approach consisted of an initial guess refinement step that captured the overall shape of the profile followed by a constrained level retrieval on predefined pressure levels.

[37] The standard deviation of the error in the estimate of the ozone profiles on a 0.8 km grid varied from 10% to 20% in the lower troposphere and 20% to 30% in the upper troposphere. The vertical resolution of the retrieval is calculated to be approximately 6 km. The vertical resolution led us to consider the time variations of ozone columns amounts in the lower and upper troposphere. The RMS error of the column is 1.34 DU in the lower troposphere and 1.37 DU in the upper troposphere. The ozone column amounts in the upper troposphere ranged from 10 and 50 DU. Based on this error analysis, TES nadir ozone retrievals should have the resolution to capture large ozone column variations in the upper troposphere such as those present in the Bermuda data set.

Appendix A. Formulation of the Nonlinear Least Squares Problem

[38] In order to determine if an estimate of an ozone profile is "close" to the true ozone profile, a measure of distance is necessary. This measure is defined by the cost function $C_{\mathrm{ML}}(\mathbf{z})$:

$$C_{\mathrm{ML}}(\mathbf{z}) = \| \mathbf{y} - \mathbf{F}(\mathbf{Mz}) \|^2_{\mathbf{S}_n^{-1}} \tag{A1}$$

where $\|\cdot\|^2_A$ is the weighted least squares norm, i.e., $\|\mathbf{x}\|^2_A = \mathbf{x}^\top \mathbf{A}\mathbf{x}$. The difference between the measurement and forward model is weighted by the measurement error covariance matrix $\mathbf{S}_n \in \mathbb{R}^{\mathrm{N}\times\mathrm{N}}$, which is defined as $\mathbf{S}_n = E(\mathbf{n}\mathbf{n}^\top)$. The cost function in equation (A1) is frequently referred to as the maximum likelihood (ML) function [*Tarantola*, 1987; *Rodgers*, 2000]. For small-residual problems, equation (A1) can be solved iteratively with the Gauss-Newton (GN) method [*Fletcher*, 1987]. The GN iterative update to the full state vector can be written as

$$\mathbf{x}_{i+1} = \mathbf{x}_i + \mathbf{M}(\mathbf{K}_i'^\top \mathbf{K}_i')^{-1}\mathbf{K}_i'^\top \mathbf{r}(\mathbf{z}_i), \tag{A2}$$

where

$$\mathbf{r}(\mathbf{z}_i) = \mathbf{S}_n^{-1/2}(\mathbf{y} - \mathbf{F}(\mathbf{Mz}_i)) \tag{A3}$$

is the weighted-residual and

$$\mathbf{K}' = \mathbf{S}_n^{-1/2}\frac{\partial \mathbf{F}(\mathbf{Mz}_i)}{\partial \mathbf{x}}\mathbf{M} \tag{A4}$$

is the weighted Jacobian.

[39] If the rank of the Jacobian is deficient or ill-determined, then the solution of equation (A1) is ill-posed and the iterations in equation (A2) may become unstable [*Hansen*, 1998]. In this case, a priori knowledge of ozone can be used to regularize the problem in order to provide a unique solution that is consistent with the data. The regularization of the inversion with a priori knowledge is implemented by augmenting the cost function in equation (A1) with an additional quadratic term:

$$C_{\mathrm{AML}}(\mathbf{z}) = \| \mathbf{y} - \mathbf{F}(\mathbf{Mz}) \|^2_{\mathbf{S}_n^{-1}} + \| \mathbf{z} - \mathbf{z}_c \|^2_{\Lambda_z} \tag{A5}$$

where $\mathbf{z}_c$ is called the constraint vector and $\Lambda_z \in \mathbb{R}^{\mathrm{M}'\times\mathrm{M}'}$ is the constraint matrix. The GN method may be applied to the minimization of equation (A5). The iterative update to the full state vector is now

$$\mathbf{x}_{i+1} = \mathbf{x}_i + \mathbf{M}\left((\mathbf{KM})\mathbf{S}_n^{-1}(\mathbf{KM})^\top + \Lambda_z\right)^{-1} \cdot \left\{(\mathbf{KM})^\top \mathbf{S}_n^{-1/2}\mathbf{r}(\mathbf{z}_i) - \Lambda_z(\mathbf{z}_i - \mathbf{z}_c)\right\} \tag{A6}$$

or

$$\mathbf{x}_{i+1} = \mathbf{x}_i + \mathbf{M}(\mathbf{K}_i''^\top \mathbf{K}_i'')^{-1}\mathbf{K}_i''^\top \mathbf{r}''(\mathbf{z}_i), \tag{A7}$$

where

$$\mathbf{r}''(\mathbf{z}) = \begin{pmatrix} \mathbf{S}_n^{-1/2}(\mathbf{y} - \mathbf{F}(\mathbf{Mz})) \\ -\Lambda_z^{1/2}(\mathbf{z} - \mathbf{z}_c) \end{pmatrix} \tag{A8}$$

is the augmented residual and

$$\mathbf{K}'' = \begin{pmatrix} \mathbf{K}' \\ \Lambda^{1/2} \end{pmatrix} \tag{A9}$$

is the augmented Jacobian.

[40] The direct calculation of equation (A2) or (A6) is generally not desirable. Rather, we solve equations (A1) or (A5) by factoring $\mathbf{K}'$ or $\mathbf{K}''$ into a QR decomposition and back-substituting for the retrieval [*Golub and Loan*, 1989].

[41] **Acknowledgments.** The research described in this paper was carried out at the Jet Propulsion Laboratory, California Institute of Technology, under a contract with the National Aeronautics and Space Administration. We would like to thank Susan Sund for assistance in calculating the climatology.

References

Beer, R., T. Glavich, and D. Rider, Tropospheric emission spectrometer for the Earth Observing System's Aura satellite, *Appl. Opt.*, *40*, 2356–2367, 2001.

Beer, R., et al., Tropospheric Emissions Spectrometer (TES) level 2 algorithm theoretical basis document, version 1.1, *D-16474*, Jet Propul. Lab., Pasadena, Calif., 1999.

Bethan, S., G. Vaughan, and S. Reid, A comparison of ozone and thermal tropopause heights and the impact of tropopause definition on quantifying the ozone content of the troposphere, *Q. J. R. Meteorol. Soc.*, *122*, 929–944, 1996.

Browell, E., et al., Large-scale air mass characteristics observed over western pacific during summertime, *J. Geophys. Res.*, *101*, 1691–1712, 1996.

Clough, S., The water vapor continuum and its role in remote sensing, *Tech. Dig. Opt. Remote Sens.*, *2*, 76–78, 1995.

Clough, S., and M. Iacono, Line-by-line calculation of atmospheric fluxes and cooling rates, 2, application to carbon-dioxide, ozone, methane, nitrous-oxide and the halocarbons, *J. Geophys. Res.*, *100*, 16,519–16,535, 1995.

Clough, S., F. Kneizys, and R. W. Davies, Line shape and the water vapor continuum, *Atmos. Res.*, *23*, 229–241, 1989.

Clough, S., C. Rinsland, and P. Brown, Retrieval of tropospheric ozone from simulations of nadir spectral radiances as observed from space, *J. Geophys. Res.*, *100*, 16,579–16,593, 1995.

Clough, S., J. Worden, P. Brown, C. Rinsland, and R. Beer, Retrieval of tropospheric ozone from simulations of limb spectral radiances as observed from space, *J. Geophys. Res.*, accepted for publication, 2002.

Crutzen, P. J., Overview of tropospheric chemistry: Developments during the past quarter century and a look ahead, in *Faraday Discussions*, pp. 1–21, 1995.

Fehsenfeld, F., P. Daum, W. Leaitch, M. Trainer, D. Parrish, and G. Hubler, Transport and processing of O-3 and O-3 precursors over the North Atlantic: An overview of the 1993 North Atlantic Regional Experiment (NARE) summer intensive, *J. Geophys. Res.*, *101*, 28,877–28,891, 1996.

Fletcher, R., *Practical Methods of Optimization*, John Wiley, New York, 1987.

Golub, G. H., and C. F. V. Loan, *Matrix Computations*, Johns Hopkins Univ. Press, Baltimore, Md., 1989.

Hansen, P. C., *Rank-Deficient and Discrete Ill-Posed Problems: Numerical Aspects of Linear Inversion*, SIAM monographs on mathematical modeling and computation, SIAM, Philadelphia, 1998.

Logan, J., An analysis of ozonesonde data for the troposphere: Recommendations for testing 3-D models and development of a gridded climatology for tropospheric ozone, *J. Geophys. Res.*, *104*, 16,115–16,149, 1999.

Merill, J., J. Moody, S. Oltmans, and H. Levy, Meteorological analysis of tropospheric ozone profiles at Bermuda, *J. Geophys. Res.*, *101*, 29,201–29,211, 1996.

Moody, J., S. Oltmans, H. Levy, and J. Merrill, Transport climatology of tropospheric ozone: Bermuda, 1998–1991, *J. Geophys. Res.*, *100*, 7179–7194, 1995.

Moody, J., et al., Meteorological mechanisms for transporting ozone over the western north Atlantic ocean: A case study for August 24–29, 1993, *J. Geophys. Res.*, *101*, 29,213–29,227, 1996.

Oltmans, S. J., et al., Summer and spring ozone profiles over the north Atlantic from ozonesonde measurements, *J. Geophys. Res.*, *101*, 29,179–29,200, 1996.

Papoulis, A., *Probability, Random Variables, and Stochastic Processes*, McGraw-Hill, New York, 1984.

Rodgers, C., *Inverse Methods for Atmospheric Sounding: Theory and Practise*, World Sci., River Edge, N. J., 2000.

Roscoe, H. K., and K. C. Clemitshaw, Measurement techniques in gas-phase tropospheric chemistry: A selective view of the past, present, and future, *Science*, *276*, 1065–1072, 1997.

Rothman, L., et al., The HITRAN molecular spectroscopic database and HAWKS (HITRAN Atmospheric Workstation): 1996 edition, *J. Quant. Spectrosc. Radiat. Transfer*, *60*, 665–710, 1998.

Singh, H. B., and D. J. Jacob, Future directions: Satellite observations of tropospheric chemistry, *Atmos. Environ.*, *34*, 4399–4401, 2000.

Steck, T., Methods for determining regularization for atmospheric retrieval problems, *Appl. Opt.*, accepted for publication, 2002.

Steck, T., and T. Clarmann, Constrained profile retrieval applied to the observation mode of the Michelson Interferometer for Passive Atmospheric Sounding, *Appl. Opt.*, *40*, 3559–3571, 2001.

Tarantola, A., *Inverse Problem Theory: Methods for Data Fitting and Model Parameter Estimation*, Elsevier Sci., New York, 1987.

Toth, R., Water vapor measurements between 590 and 2582 cm, 1, Line positions and strengths, *J. Mol. Spectrosc.*, *190*, 379–396, 1998.

Toth, R., L. Brown, and C. Plymate, Self-broadened widths and frequency shifts of water vapor lines between 590 and 2400 cm^{-1}, *J. Quant. Spectrosc. Radiat. Transfer*, *59*, 529–562, 1998.

Wang, Y. H., and D. J. Jacob, Anthropogenic forcing on tropospheric ozone and OH since preindustrial times, *J. Geophys. Res.*, *103*, 31,123–31,135, 1998.

K. Bowman, H. Worden, and J. Worden, Jet Propulsion Laboratory, California Institute of Technology, MS: 183-301, 4800 Oak Grove Dr., Pasadena, CA 91106, USA. (kevin.bowman@jpl.nasa.gov)

S. Clough, Atmospheric and Environmental Research, Cambridge, MA, USA.

C. Rodgers, Oxford University, Oxford, UK.

T. Steck, Forschungszentrum Karlsruhe, Institut für Meteorologie und Klimaforschung, Karlsruhe, Germany.